Soft Matter

PAPER

Cite this: *Soft Matter*, 2018, **14**, 5898

Splay–density coupling in semiflexible main-chain nematic polymers with hairpins

Aleksandar Popadić,[a] Daniel Svenšek,*[b] Rudolf Podgornik,[bcde] Kostas Ch. Daoulas[f] and Matej Praprotnik[ab]

Received 23rd April 2018,
Accepted 26th June 2018

DOI: 10.1039/c8sm00835c

rsc.li/soft-matter-journal

A main-chain nematic polymer melt/solution exhibits macroscopic orientational order of main polymer chains, *i.e.*, a preferred (nematic) direction. It has long been known that in such polymeric liquid crystals spatial density/concentration variations and distortions of the nematic direction are coupled, obeying a vectorial continuity constraint whose rigidity increases with chain length. Its vectorial nature precludes the application to flexible chains, where backfolds (hairpins) are present and apolar nematic symmetry is manifest, which has been its puzzling feature from the beginning. We now establish a description of the splay–density coupling in the case of arbitrary backfolding, devising a continuity constraint for the "recovered" polar order of the chain tangents and introducing hairpins as its new type of sources. Performing detailed Monte Carlo simulations of nematic monodomain melts of "soft" worm-like chains with variable length and flexibility, we show *via* their structure factors that the weakening of the coupling due to the backfolding can be consistently quantified on the macroscopic level.

1 Introduction

Formal description of line liquids[1–3] differs fundamentally from hydrodynamic description of isotropic and ordinary nematic liquids since the connectivity of the oriented lines stipulates an additional explicit macroscopic constraint.[4,5] This is true for equilibrium or living main-chain polymers, self-assembled molecular chains as well as worm-like micelles, whose consistent description implies a conservation law stemming directly from their unbroken connectivity. The exact nature and form of this conservation law proposed independently by de Gennes and Meyer, received recently a renewed scrutiny[6] that uncovered its deeper structure and important consequences missed in the previous analysis. In fact, the consequences of this conservation law trickle all the way down to fundamental macroscopic, observable properties such as structure factors and coarse-grained order parameters[7] as in, *e.g.*, the ordered and/or confined phases of DNA[8–11] or technological main-chain polymers like Kevlar fibres, Vectra and air force polymers.

In this contribution, we address the central issue of taking into account the backfolding of the polymer chain and systematically including its effects in a macroscopic conservation law. We show how such continuity equation can be articulated and how it enters the coarse-grained free energy of a nematic polymer with arbitrary chain backfolding. Specifically, we quantify the corresponding phenomenological coupling strength.[12] By comparing detailed simulations based on a recently developed mesoscopic model[13] with the predictions of the coarse-grained free-energy description augmented by the new conservation law, we derive an explicit form of the coupling strength that takes into account the nematic order as well as the density of hairpin folds.[14,15]

It has been recognized a while ago[1,2,4,5,12,16–20] that the connectivity of the polymer chain manifests itself on the macroscopic level as a constraint on the continuum fields (*i.e.*, order parameter and density/concentration) describing the coarse-grained polymer configuration. If the preferred direction is splayed (as *e.g.* when unfolding a handheld fan) in a system of long chains, Fig. 1, there are not many chain ends available to fill the so-generated voids between the chains. Consequently, the chain density decreases. For the nematic director field $\mathbf{n}(\mathbf{r})$, this constraint was written in form of a conservation law[4]

$$\nabla\cdot(\rho_s\mathbf{n}) = \rho^+ - \rho^-, \tag{1}$$

where $\rho_s(\mathbf{r})$ is the surface density or concentration of polymer chains perforating the plane perpendicular to $\mathbf{n}(\mathbf{r})$ and $\rho^+(\mathbf{r})$ and $\rho^-(\mathbf{r})$ are volume densities of the beginnings and endings of

[a] *Laboratory for Molecular Modeling, National Institute of Chemistry, SI-1001 Ljubljana, Slovenia*
[b] *Department of Physics, Faculty of Mathematics and Physics, University of Ljubljana, SI-1000 Ljubljana, Slovenia. E-mail: daniel.svensek@fmf.uni-lj.si*
[c] *Department of Theoretical Physics, J. Stefan Institute, SI-1000 Ljubljana, Slovenia*
[d] *School of Physical Sciences and Kavli Institute for Theoretical Sciences, University of Chinese Academy of Sciences, Beijing 100049, China*
[e] *CAS Key Laboratory of Soft Matter Physics, Institute of Physics, Chinese Academy of Sciences, Beijing 100190, China*
[f] *Max Planck Institute for Polymer Research, 55128 Mainz, Germany*

Fig. 1 Schematics of splay deformation. For long chains (left), the density decreases as the chains spread out, shorter chains (middle) possess more ends and can fill the voids more easily. Backfolds (right) also fill the voids, but reduce orientational ordering unless they are pointlike U turns (hairpins), which are favoured in the nematic phase. In this case, they act as chain ends and can fill the voids similar to the middle picture.

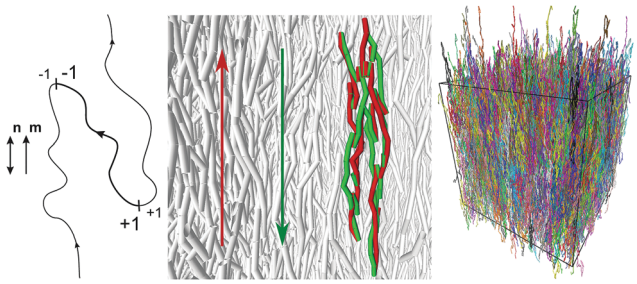

Fig. 2 Left: Pair of virtual cuts at points of folding ($\mathbf{t}\cdot\mathbf{m} = 0$) with respect to a chosen polar direction $\mathbf{m}\|\mathbf{n}$ and subsequent inversion of the backfolded ($\mathbf{t}\cdot\mathbf{m} < 0$) segments introduce a pair of separated +2 source and −2 sink, while thus-emerging polar order is independent of the folding; $\mathbf{t}$ is the unit tangent on the chain, $\mathbf{n}$ is the unit nematic preferred direction and $\mathbf{m}$ is a unit vector chosen arbitrarily in one of the two directions defined by $\mathbf{n}$ and fixed. Middle: Example of a single chain with folds (hairpins), belonging to the simulated melt (right) with 2^{18} monomers.

chains acting as sources in this continuity equation for the "polymer current" $\rho_s\mathbf{n}$.

As shown recently within a more formal framework,[6] concisely summarized in the Appendix, eqn (1) generalizes to a rigorous continuity equation for the full order vector $\mathbf{a}(\mathbf{r})$,

$$\nabla\cdot(\rho\ell_0\mathbf{a}) = \rho^+ - \rho^-, \tag{2}$$

where $\rho(\mathbf{r})$ is now the volume number density of arbitrary segments (*e.g.* monomers) of length ℓ_0; with that, $\rho_s = \rho\ell_0|\mathbf{a}|$. Eqn (2) represents a conservation law for the polymer current $\mathbf{j} = \rho\ell_0\mathbf{a}$, where it is clear by construction (see the Appendix) that $\mathbf{a}(\mathbf{r}) = \langle\mathbf{t}\rangle$ is exactly the polar order of polymer chain tangents $\mathbf{t}$. It moreover follows that eqn (1) is a special case of eqn (2) for $|\mathbf{a}|$ = const. and is therefore of the same, polar type, where $\mathbf{n}$ cannot be anything but a polar(!) preferred direction.

Notwithstanding the inconvenient fact that nematic ordering is apolar and does not exhibit a polar quantity like $\mathbf{a}$, the constraint eqn (1) has been readily applied to main-chain nematic polymers. Usually, the argument that hairpins (sharp, ideally point-like 180° turns of the chain) be absent has been invoked to circumvent the problem of the vanishing order vector and validate the use of the director $\mathbf{n}$, while it has been at the same time recognized theoretically[12,16,21–23] that hairpins act as chain ends and their density defines an effective length of the chains. Moreover, the behavior of macroscopic observables in recent simulations of polymer nematics[13] was consistent with eqn (1), provided that the influence of hairpins was not significant. For longer chains with moderate backfolding the constraint however showed weak, qualitative signs of saturation.

1.1 Recovered polar order

Recently, it has been indicated[24] that the vectorial conservation eqn (2) could be consistently applied to a nematic polymer with arbitrary number of hairpins or finite-size backfolds by introducing a so-called "recovered polar order" $\mathbf{a}^r(\mathbf{r})\|\mathbf{n}(\mathbf{r})$ of chain tangents and accompanying additional chain beginnings and endings of strength ±2 corresponding to virtual backfold cuts, Fig. 2 (left). In brief, let us assign, arbitrarily but globally, an arrow to the director (this is possible in the absence of topological disclinations) to get a nematic vector $\mathbf{m}(\mathbf{r})\|\mathbf{n}(\mathbf{r})$. Wherever a chain gets backfolded with respect to the nematic director, we make a virtual (imaginary) cut in it, thus creating a chain ending and beginning that coincide. Now we reverse those chain segments between the virtual cuts that are opposite to $\mathbf{m}$, thereby also swapping the identities of the beginnings and endings of those segments, as in Fig. 2 (left). While physically there is no change whatsoever, the result of this formal procedure is a well-defined recovered polar order $\mathbf{a}^r(\mathbf{r})\|\mathbf{m}(\mathbf{r})$ of chain tangents and new virtual beginnings (+2 sources) and endings (−2 sinks), separated in the directions upstream and downstream with respect to $\mathbf{m}$. In equilibrium, these new sources still average to zero, as do the physical beginnings (+1) and endings (−1) of the chains.

A rigorous conservation law for the recovered polar order can now be written as

$$\nabla\cdot(\rho\ell_0\mathbf{a}^r) = \Delta\rho^{s\pm}, \tag{3}$$

where the source $\Delta\rho^{s\pm} = \rho^+ - \rho^- + 2\rho^{2+} - 2\rho^{2-}$, besides mismatching physical chain ends, now contains also a contribution from mismatching densities ρ^{2+} and ρ^{2-} of up and down chain backfold virtual cuts. Here we present the first direct evidence for the relevance of this suggestion, employing extensive Monte Carlo (MC) simulations of a "soft" model of worm-like chains (WLCs)[13] and tracing the signal of the constraint eqn (3) expressed in terms of the recovered polar order $\mathbf{a}^r$. With that, we show that the semiflexibility of the polymer chain can be consistently taken into account on the macroscopic level and hairpins can be rigorously incorporated as sources in the continuity constraint on the macroscopic fields.

2 Free energy of combined sources

We first present the prerequisites needed for a lean description of the sources, which brings about a minimum number of additional parameters and does not introduce any additional variables. Such first-step asceticism is an intentional convenience and does not mean that subsequent extensions and refinements are ruled out.

Since in an apolar system there is no distinction between chain beginnings and endings (≡chain ends), we can without loss of generality consider the deviations of the densities of both of these chain end types from the equilibrium value $\rho_0^+ = \rho_0^- \equiv \frac{1}{2}\rho_0^\pm$ to be symmetric,†

$$\rho^+ - \rho_0^+ = -\left(\rho^- - \rho_0^-\right) \equiv \frac{1}{2}\Delta\rho^\pm, \tag{4}$$

$$\rho^{2+} - \rho_0^{2+} = -\left(\rho^{2-} - \rho_0^{2-}\right) \equiv \frac{1}{2}\Delta\rho^{2\pm}, \tag{5}$$

where an analogous statement, eqn (5), holds for up and down backfolds with the equilibrium density $\rho_0^{2+} = \rho_0^{2-} \equiv \frac{1}{2}\rho_0^{2\pm}$. This does not imply in any way that the number of backfolds per chain should be even. It just reflects the symmetry-based facts that (i) in a homogeneous equilibrium system the number of up and down backfolds is equal on average, that (ii) the deviations $\rho^{2+} - \rho_0^{2+}$ and $\rho^{2-} - \rho_0^{2-}$ from the homogeneous distributions are equally costly, (iii) that in the source of the continuity equation, eqn (3), $\rho^{2+} - \rho_0^{2+}$ is equivalent to $-(\rho^{2-} - \rho_0^{2-})$ (excess of up backfolds has the same effect as shortfall of down backfolds), and (iv) that we will not distinguish between these two types of sources. As long as $\Delta\rho^{2\pm}$ is much smaller than $\rho_0^{2\pm}$, this distinction plays no role.

Describing the chain ends and the backfold cuts as two types of free noninteracting particles (two ideal gases), the free-energy cost of their nonequilibrium distribution is entropic,[1]

$$\Delta f\left(\Delta\rho^\pm, \Delta\rho^{2\pm}\right) = \frac{k_\mathrm{B}T}{2}\left[\frac{\left(\Delta\rho^\pm\right)^2}{\rho_0^\pm} + \frac{\left(\Delta\rho^{2\pm}\right)^2}{\rho_0^{2\pm}}\right]. \tag{6}$$

We want to treat both types of particles on an equal basis and describe the source in eqn (3) by the single variable

$$\Delta\rho^{s\pm} = \Delta\rho^\pm + 2\Delta\rho^{\pm 2}, \tag{7}$$

without considering its breakdown into the two individual contributions. Only in this case the constraint eqn (3) can be taken into account simply by a penalty potential term in the free energy. If one wants to go beyond that, $\Delta\rho^\pm$ and $\Delta\rho^{\pm 2}$ must be considered as additional system variables with the free energy cost eqn (6), while eqn (3) is an additional equation besides that of the free-energy minimization. Including in this case also a general free-energy coupling of both source densities to existing system variables is natural, but already highly detailed.

Considering combined sources, the free-energy density of the total source $\Delta\rho^{s\pm}$ is obtained by averaging eqn (6) over all possible realizations eqn (7) of $\Delta\rho^{s\pm}$:

$$\begin{aligned}\Delta\bar{f}\left(\Delta\rho^{s\pm}\right) = &\iint_{-\infty}^{\infty} \mathrm{d}\Delta\rho^\pm \mathrm{d}\Delta\rho^{p\pm} \Delta f\left(\Delta\rho^\pm, \Delta\rho^{p\pm}\right) \\ &\times \mathscr{P}\left(\Delta\rho^\pm\right)\mathscr{P}\left(\Delta\rho^{p\pm}\right)\delta\left(\Delta\rho^\pm + p\Delta\rho^{p\pm} - \Delta\rho^{s\pm}\right),\end{aligned} \tag{8}$$

with $\Delta\rho^{p\pm} \equiv \Delta\rho^{2\pm}$ and $p(=2)$ introduced for trackability. Here

$$\mathscr{P}\left(\Delta\rho^\pm\right) \propto \mathrm{e}^{-\frac{V_1\left(\Delta\rho^\pm\right)^2}{2\rho_0^\pm}} \tag{9}$$

and analogously for $P(\Delta\rho^{p\pm})$, V_1 is an arbitrary volume (*e.g.* the coarse-graining volume) not appearing in the final result and the normalization is

$$\begin{aligned}1 = &\iint_{-\infty}^{\infty} \mathrm{d}\Delta\rho^\pm \mathrm{d}\Delta\rho^{p\pm} \mathscr{P}\left(\Delta\rho^\pm\right)\mathscr{P}\left(\Delta\rho^{p\pm}\right) \\ &\times \delta\left(\Delta\rho^\pm + p\Delta\rho^{p\pm} - \Delta\rho^{s\pm}\right).\end{aligned} \tag{10}$$

The result of the integration eqn (8) is

$$\Delta\bar{f}\left(\Delta\rho^{s\pm}\right) = \frac{k_\mathrm{B}T}{2}\left(\frac{1}{V_1} + \frac{\left(\Delta\rho^{s\pm}\right)^2}{\rho_0^\pm + p^2\rho_0^{p\pm}}\right), \tag{11}$$

where the first, constant term $k_\mathrm{B}T/(2V_1)$ can be omitted—it arises due to the fact that the state $\Delta\rho^{s\pm} = 0$ can be realized by $\Delta\rho^\pm = -p\Delta\rho^{p\pm} \neq 0$, which costs energy.

The average free-energy density of the total source $\Delta\rho^{s\pm}$ is thus

$$\Delta\bar{f}\left(\Delta\rho^{s\pm}\right) = \frac{k_\mathrm{B}T}{2}\frac{\left(\Delta\rho^{s\pm}\right)^2}{\rho_0^\pm + 4\rho_0^{2\pm}} \equiv \frac{1}{2}G\left(\Delta\rho^{s\pm}\right)^2 \tag{12}$$

and presents a penalty potential with strength G of the continuity constraint eqn (3) for the recovered polar order. We note again that this is the leanest possible treatment of the sources that however takes into account both chain ends $\Delta\rho^\pm$ as well as chain backfolds $\Delta\rho^{2\pm}$. In this minimal picture, they are merged into a single source, $\Delta\rho^{s\pm}$. The key implication is the weighted composition of the effective susceptibility $G \propto 1/(\rho_0^\pm + 4\rho_0^{2\pm})$ from the equilibrium densities, where the contribution of the backfolds $\rho_0^{2\pm}$ is $(\pm 2)^2 = 4$ times that of the ends $\rho_0^\pm$.

Note that in the limit of noninteracting chain ends the distribution of chain lengths is irrelevant—it is just the density of chain ends $\rho_0^\pm$ that matters. Only for monodisperse chains with N_s segments we have simply $\rho_0^\pm = 2\rho/N_\mathrm{s}$. Naturally, broadening the distribution of N_s at fixed $\rho_0^\pm$ and ρ will increase the density of backfolds $\rho_0^{2\pm}$ (unless the persistence length is either very large or very small compared to the chain lengths) and will thus weaken the constraint according to eqn (12). Determining $\rho_0^{2\pm}$ is, however, a separate problem, whereas for the presented macroscopic description $\rho_0^{2\pm}$ is a parameter. In fact, the strength of the constraint is a macroscopic probe of the density of microscopic chain backfolds.

† This is a trivial statement. In a nematic, there can be no physical distinction between beginnings and endings. Moreover, the arbitrary choice of the direction of chain parametrization cannot influence any physical configuration whatsoever: selecting at random a chain end anywhere in the system, under any condition, there is no preference towards a beginning or ending. In a nematic, ρ^+ and ρ^- are not separate variables. There is only one variable, $\Delta\rho^\pm$.

3 Macroscopic description of fluctuations

We neglect fluctuations of the nematic order modulus and expand the coarse-grained segment density $\rho = \rho_0 + \delta\rho(\mathbf{q})$ and director $\mathbf{n} = \mathbf{n}_0 + \delta\mathbf{n}(\mathbf{q})$ fields around their equilibrium values ρ_0, $\mathbf{n}_0$. Since $|\mathbf{n}|^2 = 1$, the director fluctuations $\delta\mathbf{n}$ are orthogonal to $\mathbf{n}_0$. Conforming to the uniaxial symmetry, the Fourier space is set up as $\mathbf{q} = \mathbf{q}_\perp + q_\parallel\mathbf{n}_0$, where $\mathbf{q}_\perp$ is an arbitrary direction perpendicular to $\mathbf{n}_0$. The free-energy[1,7] contribution of a Fourier mode in the volume V is $F_\mathbf{q} = f(\mathbf{q})/V$ and

$$\begin{aligned} f(\mathbf{q}) &= \frac{1}{2}\tilde{G}\left|q_\parallel\frac{\delta\rho}{\rho_0} + q_\perp\delta n_\mathrm{L}\right|^2 + \frac{1}{2}B\left|\frac{\delta\rho}{\rho_0}\right|^2 \\ &\quad + \frac{1}{2}\left(K_1 q_\perp{}^2 + K_3 q_\parallel{}^2\right)|\delta n_\mathrm{L}|^2 \\ &\quad + \frac{1}{2}\left(K_2 q_\perp{}^2 + K_3 q_\parallel{}^2\right)|\delta n_\mathrm{T}|^2, \end{aligned} \tag{13}$$

where δn_L, δn_T are the longitudinal (lying in the plane defined by $\mathbf{n}_0$ and $\mathbf{q}_\perp$) and transverse components with respect to $\mathbf{q}_\perp$, B is the compressibility modulus and $K_{\{1,2,3\}}$ are the {splay,twist,bend} elastic constants. The first term of eqn (13) is exactly the free-energy cost eqn (12) of the total source $\Delta\rho^{s\pm}$, expressed by the left-hand side of the conservation law eqn (3) for the recovered polar order; here $\tilde{G} = G(\rho_0\ell_0 a_0^r)^2$ and a_0^r is the equilibrium magnitude of the recovered polar order.

The theoretical structure factor of the coarse-grained system $S(\mathbf{q}) = \langle\delta\rho(\mathbf{q})\delta\rho(-\mathbf{q})\rangle/N$, where N is the total number of ℓ_0 segments, corresponding to the free-energy eqn (13) is then found to be[1,7]

$$S(\mathbf{q}) = k_\mathrm{B}T\rho_0\frac{q_\perp{}^2 + \left(K_1 q_\perp{}^2 + K_3 q_\parallel{}^2\right)/\tilde{G}}{Bq_\perp{}^2 + \left(B/\tilde{G} + q_\parallel{}^2\right)\left(K_1 q_\perp{}^2 + K_3 q_\parallel{}^2\right)}, \tag{14}$$

while the longitudinal director fluctuation $D_\mathrm{L}(\mathbf{q}) = \langle\delta n_\mathrm{L}(\mathbf{q})\delta n_\mathrm{L}(-\mathbf{q})\rangle/N$ is[1,7]

$$D_\mathrm{L}(\mathbf{q}) = \frac{k_\mathrm{B}T}{\rho_0}\frac{q_\parallel{}^2 + B/\tilde{G}}{Bq_\perp{}^2 + \left(B/\tilde{G} + q_\parallel{}^2\right)\left(K_1 q_\perp{}^2 + K_3 q_\parallel{}^2\right)}. \tag{15}$$

The dependence of the structure factor eqn (14) on the reduced susceptibility $\tilde{G}$ makes it a suitable signal for detecting the constraint eqn (3) and determining its strength from molecular simulation data, Fig. 3. The comparison is restricted to the region of low $\mathbf{q}$ (on the scale of the monomer size), where microscopic simulation and coarse-grained theory should agree.

4 Mesoscopic WLC model and simulations

Validating the predictions of the macroscopic theory with molecular-level computer simulations of polymer nematics[25,26] is challenging, since such simulations must (i) address the long-wavelength limit and (ii) realize different regimes of chain backfolding (hairpin formation). Thus, it is essential to consider large systems containing long polymer chains.[27] We fulfill these

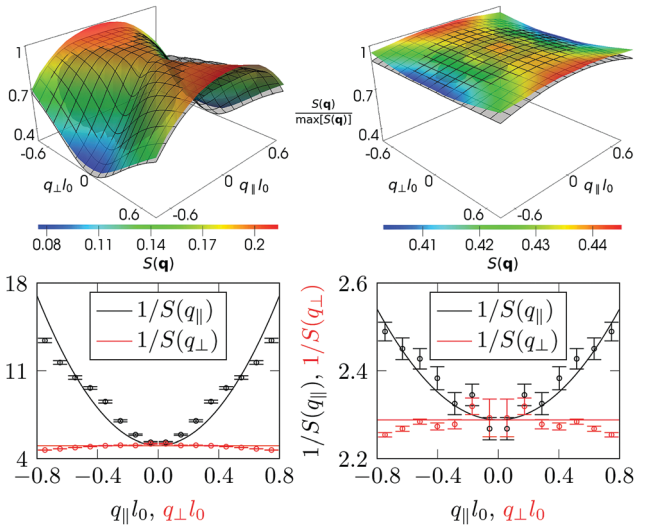

Fig. 3 Top: Structure factors $S(q_\perp l_0, q_\parallel l_0)$ calculated in simulations (solid), scaled to their maximum values and fitted (wireframe) by eqn (14), for stiff (left column) and flexible (right column) chains of length $128l_0$; l_0 is the length of the WLC segment. Bottom: Cross sections of S^{-1} for $q_\perp = 0$ (black) and $q_\parallel = 0$ (red).

requirements benefiting from a recently developed mesoscopic model[13] which describes the polymers as discrete WLCs, Fig. 2 (middle, right).

The modeled system contains N_c monodisperse WLCs comprised of N_s linearly connected segments of fixed length l_0. Consecutive segments are subjected to a standard angular potential $U_\mathrm{b} = -\varepsilon\mathbf{u}^i(s)\cdot\mathbf{u}^i(s+1)$, where $\mathbf{u}^i(s)$ is the unit vector along the s-th segment of the i-th chain and ε controls the WLC bending stiffness. Non-bonded interactions between segments are introduced *via* the potential $U_\mathrm{nb} = U(r^{ij}(s,t))[\kappa - (2\nu/3)\mathbf{q}^i(s):\mathbf{q}^j(t)]$, where $U(r^{ij}(s,t)) = C_0\Theta(2\sigma - r^{ij}(s,t))[4\sigma + r^{ij}(s,t)][2\sigma - r^{ij}(s,t)]^2$ and $r^{ij}(s,t)$ is the distance between the centers of the s-th and t-th segments of the i-th and j-th chain, respectively. The interaction range is controlled by σ as indicated by the Heaviside function Θ. To validate the predictions of the macroscopic theory it is sufficient to employ a generic model with a single "microscopic" length scale. Hence, we set $\sigma = l_0$, although other choices are possible[28,29] when modeling actual materials. The integrated strength of $U(r^{ij}(s,t))$ is normalized to ${l_0}^3$, choosing $C_0 = 3{l_0}^3/(64\pi\sigma^6)$. The strength of the isotropic repulsion between the segments is controlled by the parameter κ. Nematic alignment is promoted by the anisotropic part of U_nb, which depends on the inner product of tensors $\mathbf{q}^i(s) = [3\mathbf{u}^i(s) \otimes \mathbf{u}^i(s) - \mathbf{I}]/2$ quantifying the segmental orientation in the laboratory frame. The strength of these Maier–Saupe-like interactions is controlled by ν.

Two molecular flexibilities $\varepsilon = 0$ and $\varepsilon = 3.284k_\mathrm{B}T$ are addressed, corresponding to flexible and stiff chains, respectively. In both cases, we consider WLCs with $N_\mathrm{s} = \{32,64,128\}$ segments. We empirically set $\kappa = 7.58k_\mathrm{B}T$, while $\nu = 3.33k_\mathrm{B}T$ and $6.66k_\mathrm{B}T$ for the stiff and flexible chains, respectively. For this κ, the repulsive interactions are strong enough to furnish a stable polymer liquid (positive compressibility[28]) but remain sufficiently "soft" for efficient simulations. Our choices of ν lead to stable and

sufficiently deep nematic order in the entire range of considered stiffness parameters: the moduli of the uniaxial quadrupolar order are $S = \{0.652,0.668,0.678\}$ and $S = \{0.840,0.842,0.842\}$ for stiff and flexible chains with $N_s = \{32,64,128\}$, respectively, while the corresponding moduli of the recovered polar order are $a_0^r = \{0.865,0.872,0.876\}$ and $a_0^r = \{0.943,0.944,0.944\}$; all standard errors are below 0.05%.

We study large nematic monodomains containing $N = N_c N_s = 2^{18}$ segments, Fig. 2 (right). They are equilibrated through MC starting from configurations where all chains are stretched and aligned along the z-axis of the laboratory frame, having their centers-of-mass randomly distributed. The MC algorithm utilizes standard[30,31] slithering-snake moves, as well as volume fluctuation moves at pressure $Pl_0^3/(k_BT) = 2.87$ resulting in system's volume fluctuations of $\sim$1%. While working in the isothermal–isobaric ensemble is computationally more expensive, it is preferred to exclude isotropic/nematic coexistence in the entire range of considered parameters.

Since the global nematic direction and the ensemble volume are free to fluctuate, we compute the structure factor $S(q_x,q_y,q_z)$ of each configuration in the laboratory frame and assign it to a bin representing $S(q_\perp,q_\parallel)$, where $q_\parallel$ and $q_\perp = |\mathbf{q}_\perp|$ are the components parallel and orthogonal to the current nematic director determined as the principal eigenvector of $(1/N)\sum_{i,s}\mathbf{q}^i(s)$. With that, $S(q_\perp,q_\parallel)$ is computed in the director-based 123 frame.[13,32,33] The principal eigenvector is also used to determine, for each configuration, the modulus of the recovered polar order a_0^r appearing in the definition of $\tilde{G}$, which is then averaged over all recorded configurations. The same is done for the density of segments $\rho_0 = N/\langle V\rangle$ (putting $\ell_0 = l_0$) in eqn (14), as well as the densities of chain ends $\rho_0^{\pm}$ and backfolds $\rho_0^{2\pm}$ in eqn (12). In all cases, block-averaging with block size τ is employed, where τ is the number of MC steps needed to decorrelate the end-to-end vector of the WLC. Computationally most severe are stiff chains with $N_s = 128$ segments, where τ was as high as 130 000 and a MC sequence of 48τ was reached. In other cases the runs in terms of τ were longer.

5 Results & discussion

Large sequences of nematic melt monodomain configurations, accumulated using the efficient soft model, allow for direct validation[34] of the macroscopic theory *via* the structure factor eqn (14). We compute[13] also the longitudinal director fluctuation $D_L(\mathbf{q}) = \langle \delta n_L(\mathbf{q})\delta n_L(-\mathbf{q})\rangle/N$, eqn (15). For stiff chains, where the constraint eqn (3) is expectedly strong, D_L shows a characteristic strengthening[1,13] of the effective splay (K_1) elastic constant, Fig. 4.

The computed $S(q_\perp,q_\parallel)$ and $D_L(q_\perp,q_\parallel)$ landscapes, Fig. 3 and 4, are fitted with the theoretical expressions eqn (14) and (15) to extract the parameters B, $\tilde{G}$, K_1, K_3. Fig. 3 (bottom) shows cross sections of the two-dimensional structure factor fits. For small wave vectors it is verified that $S^{-1}(0,q_\parallel)$ is parabolic, while $S^{-1}(q_\perp,0)$ is essentially constant, as predicted by eqn (14). The kinks at $q_\parallel l_0 \approx \pm 0.5$ are attributed to microscopic effects not captured by the macroscopic theory, *e.g.* enhanced correlations within single chains or groups of neighboring chains.[35]

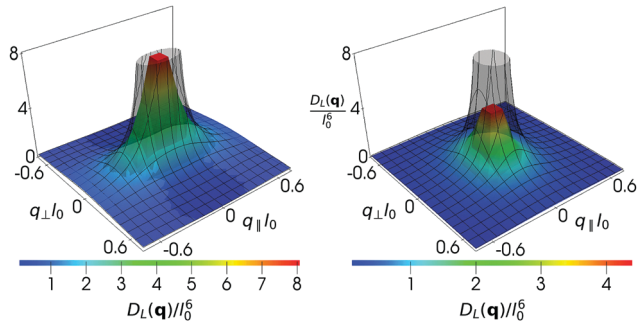

Fig. 4 Longitudinal director fluctuations $D_L(q_\perp l_0,q_\parallel l_0)$ calculated in simulations (solid), fitted (wireframe) by eqn (15), for stiff (left) and flexible (right) chains of length $128l_0$.

Using averaged values ρ_0 and a_0^r, the strength G of the constraint is determined from the fitting parameter $\tilde{G}$ and is plotted in dimensionless form in Fig. 5 as a function of the dimensionless inverse density of chain ends/backfolds as suggested by eqn (12). The average numbers of backfolds per chain are $\{0.33,0.58,1.1\}$ and $\{11.9,24.0,48.2\}$ for stiff and flexible chains with $N_s = \{32,64,128\}$, respectively. The direct comparison with the theoretical line, not involving any fitting parameter, confirms the relevance of the prediction eqn (12), while the agreement of the slopes is especially notable. Moreover, the points corresponding to the flexible chains in Fig. 5 (inset) show a highly reduced splay–density coupling, thus confirming the concept of the recovered polar order and the applicability of the conservation law eqn (3) formulated on its basis, as well as the role of backfolds as sources in this conservation law.

It is hard to overlook the hinted offset of the simulated stiff chain points from the theoretical solid line in Fig. 5. We interpret it as a deviation from the noninteracting gas idealization of the

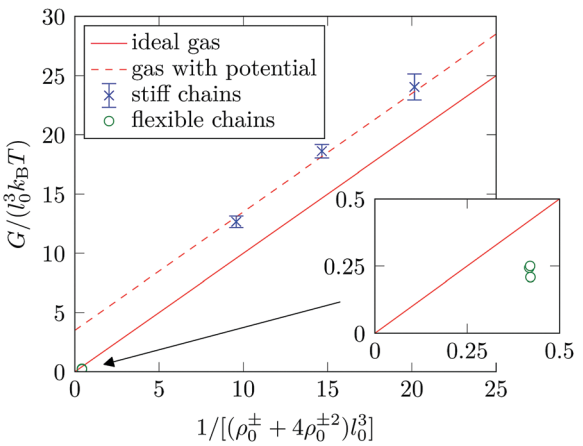

Fig. 5 Dimensionless strength of the constraint $G = \tilde{G}/(\rho_0 l_0 q_0)^2$, determined from the fits of the MC structure factor landscapes Fig. 3, *versus* the dimensionless inverse density of the combined sources (solid line, no fitting parameter). Following eqn (19), an offset (dashed line) is fitted to the three points representing the stiff chains with $N_s = \{32,64,128\}$.

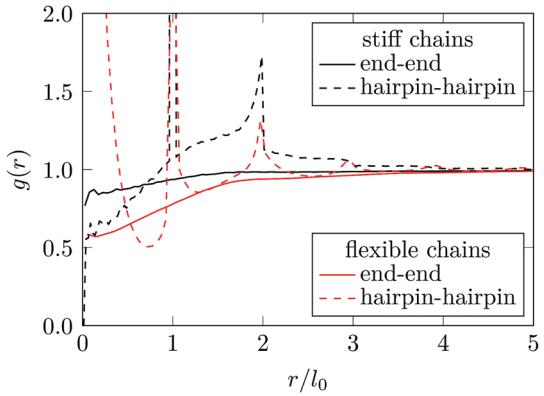

Fig. 6 RDFs of chain ends and backfolds (hairpins) for stiff (black) and flexible (red) chains with $N_s = 128$ obtained in simulations. The end–hairpin RDFs (not shown) are qualitatively similar to the hairpin–hairpin RDFs.

chain ends/backfolds (≡particles). It is clear that at least the intra-chain backfolds of near segments are not independent. In fact, the computed end–end, hairpin–hairpin and end–hairpin radial distribution functions (RDFs), Fig. 6, show deviations of various kinds from the ideal gas behavior $g(r) = 1$ for $r \lessapprox 3l_0$. The end–end RDFs manifest simple repulsion. In contrast, the hairpin–hairpin RDFs have a complex structure due to contributions from hairpins on the same chain: small distances between sequential backfolds along the chain can assume only specific values, which explains the pronounced spikes (even for the stiff WLCs). Such small-scale effects, as well as distinguishing between intra- and intermolecular backfolds in eqn (12), are beyond the scope of the present macroscopic theory.

It is, however, sensible to capture the interactions between the particles by an effective free-energy density $f(\rho^{s\pm})$ of the particle distribution $\rho^{s\pm}$,

$$f\left(\rho^{s\pm}\right) = k_B T \rho^{s\pm} \ln \frac{\rho^{s\pm}}{C} + \frac{1}{2} A \left(\rho^{s\pm}\right)^2, \tag{16}$$

where the pair-interaction free-energy density is proportional to $(\rho^{s\pm})^2$ by definition, while all details of this interaction are contained in a phenomenological second virial coefficient A; $A > 0$ stands for an effective repulsion. The first derivative $p_0 = -V'\partial f/\partial V = \rho\partial f/\partial\rho$ determines the "osmotic pressure" p_0 required to maintain an equilibrium density $\rho_0^{s\pm}$ of particles. In other words, $\dfrac{\partial H}{\partial V} = 0$ holds in equilibrium, where $H = V'f + p_0 V$ is the Gibbs free energy. Here V' represents the volume of an arbitrary portion (as does V), but (unlike V) is not included in the differentiation since the number of particles within the portion is considered fixed. Thence, keeping $V' = V$ constant, the expansion of H for a nonequilibrium distribution $\Delta\rho^{s\pm}(\mathbf{r}) = \rho^{s\pm}(\mathbf{r}) - \rho_0^{s\pm}$ within the portion is

$$\Delta H = V'\Delta f = V' \frac{\partial f}{\partial \rho^{s\pm}}\bigg|_{\rho_0^{s\pm}} \Delta\rho^{s\pm} + V' \frac{1}{2} \frac{\partial^2 f}{\partial (\rho^{s\pm})^2}\bigg|_{\rho_0^{s\pm}} \left(\Delta\rho^{s\pm}\right)^2. \tag{17}$$

Since the spatial average of $\Delta\rho^{s\pm}$ is zero, the linear term vanishes and we have

$$\Delta f\left(\Delta\rho^{s\pm}\right) = \frac{1}{2} \frac{\partial^2 f}{\partial (\rho^{s\pm})^2}\bigg|_{\rho_0^{s\pm}} \left(\Delta\rho^{s\pm}\right)^2. \tag{18}$$

Considering in eqn (18) only the first, entropic contribution in eqn (16), the nonequilibrium ideal gas expressions eqn (6) follow. Taking into account also the second, interaction contribution of eqn (16), we finally get

$$\Delta f\left(\Delta\rho^{s\pm}\right) = \frac{1}{2}\left(\frac{k_B T}{\rho_0^{s\pm}} + A\right)\left(\Delta\rho^{s\pm}\right)^2, \tag{19}$$

which would explain the rather constant positive offset ($A > 0$) of $G(1/\rho_0^{s\pm})$ observed in Fig. 5 (dashed line) for the set of stiff chains. This repulsive effective interaction makes nonequilibrium excursions $\Delta\rho^{s\pm}$ more expensive, eqn (19), and hence the constraint eqn (3) is stronger. Note, however, that the strength A of the effective interaction depends on the composition of the particle gas, *i.e.*, the ratio $\rho_0^{2\pm}/\rho_0^{\pm}$, and furthermore that also the RDFs depend on N_s and other parameters.

6 Conclusion

In summary, we have established a consistent macroscopic description of the splay–density coupling in semiflexible main-chain nematic polymers with hairpins, using a vectorial continuity constraint for the recovered polar order of chain tangents and introducing chain backfolds as its new type of sources besides chain ends. In the minimal spirit, we unified both types of sources to a mixture of two ideal gases with fixed composition. Conducting detailed Monte Carlo simulations of nematic monodomain melts of worm-like chains with variable length and flexibility, we demonstrated that the chain backfolding weakens the splay–density coupling. We showed how this weakening can be quantified on the macroscopic level by connecting the strength of the coupling with the macroscopic equilibrium densities of chain ends and backfolds. Refinements and ramifications of this first description are possible in various directions. The possibility of virial corrections has been briefly illuminated. They can be introduced for each type of sources separately to take into account its empirical specifics, in particular the effective interaction between the backfolds of the same chain and an anticipated direct influence of the bending rigidity of the chain on this interaction. It is also possible to introduce the sources as one or more additional field variables and couple them in a phenomenological spirit to the existing system variables by general symmetry-allowed coupling terms.

Conflicts of interest

There are no conflicts to declare.

Appendix

A Vectorial conservation law

Define the microscopic worm-like chain tangent field

$$j_i^{\mathrm{mic}}(\mathbf{x}) = \sum_\alpha \int_{\mathbf{x}^\alpha(s)} \mathrm{d}s\, \delta(\mathbf{x} - \mathbf{x}^\alpha(s)) t_i(s), \tag{20}$$

where $\mathbf{x}^\alpha(s)$ is the continuous contour of chain α in natural parametrization and $\mathbf{t}(s) = \mathrm{d}\mathbf{x}^\alpha(s)/\mathrm{d}s$ is the unit tangent on the chain. For brevity we will be omitting the superscript α and the sum $\sum_\alpha$ over the chains. Taking the divergence of eqn (20) and transforming it stepwise, we get

$$\begin{aligned} \partial_i j_i^{\mathrm{mic}}(\mathbf{x}) &= \int_{\mathbf{x}(s)} \mathrm{d}s \frac{\mathrm{d}x_i(s)}{\mathrm{d}s} \frac{\partial}{\partial x_i} \delta(\mathbf{x} - \mathbf{x}(s)) \\ &= -\int_{\mathbf{x}(s)} \mathrm{d}s \frac{\mathrm{d}x_i(s)}{\mathrm{d}s} \frac{\partial}{\partial x_i(s)} \delta(\mathbf{x} - \mathbf{x}(s)) \\ &= -\int_{\mathbf{x}(s)} \mathrm{d}s \frac{\mathrm{d}}{\mathrm{d}s} \delta(\mathbf{x} - \mathbf{x}(s)) \\ &= \delta(\mathbf{x} - \mathbf{x}(0)) - \delta(\mathbf{x} - \mathbf{x}(L)), \end{aligned} \tag{21}$$

where L is the length of the chain.

Coarse-graining (denoted by $\overline{}$) the microscopic field eqn (20) to a mesoscopic volume V_0 centered at $\mathbf{x}$ gives the corresponding mesoscopic field

$$\begin{aligned} \mathbf{j}(\mathbf{x}) &= \overline{\mathbf{j}^{\mathrm{mic}}}(\mathbf{x}) = \frac{1}{V_0} \int_{V_0(\mathbf{x})} \mathrm{d}^3x'\, \mathbf{j}^{\mathrm{mic}}(\mathbf{x}') \\ &= \frac{1}{V_0} \int_{\mathbf{x}(s) \in V_0(\mathbf{x})} \mathrm{d}s\, \mathbf{t}(s) \\ &= \frac{L(\mathbf{x})}{V_0} \frac{1}{L(\mathbf{x})} \int_{\mathbf{x}(s) \in V_0(\mathbf{x})} \mathrm{d}s\, \mathbf{t}(s), \end{aligned} \tag{22}$$

where $L(\mathbf{x}) = \int_{\mathbf{x}(s) \in V_0(\mathbf{x})} \mathrm{d}s \equiv N(\mathbf{x})\ell_0$ is the total length of the chain within the volume V_0, which can be expressed in terms of an arbitrary segment length ℓ_0 and the number N of these segments within the volume. Hence, the mesoscopic field can be written as

$$\mathbf{j}(\mathbf{x}) = \rho(\mathbf{x})\ell_0 \mathbf{a}(\mathbf{x}), \tag{23}$$

where $\rho(\mathbf{x}) = N(\mathbf{x})/V_0$ is the mesoscopic volume number density of the segments and

$$\mathbf{a}(\mathbf{x}) = \frac{1}{L(\mathbf{x})} \int_{\mathbf{x}(s) \in V_0(\mathbf{x})} \mathrm{d}s\, \mathbf{t}(s) \tag{24}$$

is the mesoscopic average of $\boldsymbol{t}(s)$, *i.e.*, the polar order of polymer chain tangents.

We apply this coarse-graining procedure to eqn (21) and take into account that ∇ and coarse-graining commute, *i.e.*, $\overline{\partial_i j_i^{\mathrm{mic}}} = \partial_i \overline{j_i^{\mathrm{mic}}} = \partial_i j_i$. The result is an equation for the continuum mesoscopic field—the vectorial conservation law

$$\nabla \cdot \mathbf{j} = \nabla \cdot (\rho \ell_0 \mathbf{a}) = \rho^+ - \rho^-, \tag{25}$$

where $\rho^+(\mathbf{x}) = \overline{\delta(\mathbf{x} - \mathbf{x}(0))}$, $\rho^-(\mathbf{x}) = \overline{\delta(\mathbf{x} - \mathbf{x}(L))}$ are mesoscopic densities of beginnings and endings of the chains.

Acknowledgements

We are grateful to Patrick Gemünden and Gregor Skačej for useful discussions. The support of the Slovenian Research Agency—Grants P1-0002, P1-0055, J1-7435, J1-7441 is gratefully acknowledged.

References

1 D. R. Nelson, *Phys. A*, 1991, **177**, 220–232.
2 R. D. Kamien and D. R. Nelson, *J. Stat. Phys.*, 1993, **71**, 23–50.
3 D. R. Nelson, *Defects and Geometry in Condensed Matter Physics*, Cambridge University Press, Cambridge, 2002.
4 P. G. de Gennes, *Mol. Cryst. Liq. Cryst.*, 1976, **34**, 177–182.
5 R. B. Meyer, *Polymer Liquid Crystals*, Academic Press, New York, 1982, pp. 133–163.
6 D. Svenšek, G. M. Grason and R. Podgornik, *Phys. Rev. E: Stat., Nonlinear, Soft Matter Phys.*, 2013, **88**, 052603.
7 D. Svenšek and R. Podgornik, *J. Chem. Phys.*, 2015, **143**, 114902.
8 H. Shin and G. M. Grason, *EPL*, 2011, **96**, 36007.
9 D. Svenšek, G. Veble and R. Podgornik, *Phys. Rev. E: Stat., Nonlinear, Soft Matter Phys.*, 2010, **82**, 011708.
10 J. Zavadlav, R. Podgornik and M. Praprotnik, *Sci. Rep.*, 2017, **7**, 4775.
11 R. Podgornik, J. Zavadlav and M. Praprotnik, *Computation*, 2018, **6**, 3.
12 R. D. Kamien, P. Le Doussal and D. R. Nelson, *Phys. Rev. A: At., Mol., Opt. Phys.*, 1992, **45**, 8727–8750.
13 P. Gemünden and K. C. Daoulas, *Soft Matter*, 2015, **11**, 532–544.
14 M. H. Li, A. Brûlet, P. Davidson, P. Keller and J. P. Cotton, *Phys. Rev. Lett.*, 1993, **70**, 2297–2300.
15 M. H. Li, A. Brûlet, J. P. Cotton, P. Davidson, C. Strazielle and P. Keller, *J. Phys. II*, 1994, **4**, 1843–1863.
16 G. J. Vroege and T. Odijk, *Macromolecules*, 1988, **21**, 2848–2858.
17 X. Ao, X. Wen and R. B. Meyer, *Phys. A*, 1991, **176**, 63–71.
18 J. V. Selinger and R. F. Bruinsma, *Phys. Rev. A: At., Mol., Opt. Phys.*, 1991, **43**, 2910–2921.
19 P. L. Doussal and D. R. Nelson, *EPL*, 1991, **15**, 161.
20 J. V. Selinger and R. F. Bruinsma, *J. Phys. II*, 1992, **2**, 1215–1236.
21 R. G. Petschek and E. M. Terentjev, *Phys. Rev. A: At., Mol., Opt. Phys.*, 1992, **45**, 930–938.
22 T. Odijk, *J. Chem. Phys.*, 2006, **125**, 204904.
23 T. Odijk, *Phys. Rev. E: Stat., Nonlinear, Soft Matter Phys.*, 2008, **77**, 060901.
24 D. Svenšek and R. Podgornik, *Phys. Rev. E*, 2016, **93**, 052703.
25 L. Delle Site and M. Praprotnik, *Phys. Rep.*, 2017, **693**, 1–56.
26 M. Praprotnik, L. D. Site and K. Kremer, *Annu. Rev. Phys. Chem.*, 2008, **59**, 545–571.
27 K. Kremer and G. S. Grest, *J. Chem. Phys.*, 1990, **92**, 5057–5086.

28 K. C. Daoulas, V. Rühle and K. Kremer, *J. Phys.: Condens. Matter*, 2012, **24**, 284121.
29 C. Greco, Y. Jiang, J. Z. Y. Chen, K. Kremer and K. C. Daoulas, *J. Chem. Phys.*, 2016, **145**, 184901.
30 D. Frenkel and B. Smit, *Understanding Molecular Simulation: From Algorithms to Applications*, Academic Press, San Diego, 2nd edn, 2001.
31 M. Tuckerman, *Statistical Mechanics: Theory and Molecular Simulation*, Oxford University Press, Oxford, 2010.
32 M. P. Allen, M. A. Warren, M. R. Wilson, A. Sauron and W. Smith, *J. Chem. Phys.*, 1996, **105**, 2850–2858.
33 P. A. O'Brien, M. P. Allen, D. L. Cheung, M. Dennison and A. Masters, *Phys. Rev. E: Stat., Nonlinear, Soft Matter Phys.*, 2008, **78**, 051705.
34 O. Pelletier, C. Bourgaux, O. Diat, P. Davidson and J. Livage, *Eur. Phys. J. E: Soft Matter Biol. Phys.*, 2000, **2**, 191–198.
35 S. A. Egorov, A. Milchev and K. Binder, *Phys. Rev. Lett.*, 2016, **116**, 187801.